The Stochastic Multi-cloud Model (SMCM) convective parameterization in the CFSv2 : Scopes and Opportunities

B. B. Goswami[1], B Khouider[1], R Phani[2], P Mukhopadhyay[2], and A.J. Majda[3,4]

[1]Department of Mathematics and Statistics, University of Victoria, BC, Canada.

[2]Indian Institute of Tropical Meteorology, Pune, India

[3]Department of Mathematics and Center for Atmosphere and Ocean Sciences, Courant Institute for Mathematical Sciences, New York University, New York, USA

[4]Center for Prototype Climate Models, New York University-Abu Dhabi, Abu Dhabi, United Arab Emirates

Corresponding author: B. B. Goswami, bgoswami@uvic.ca

Abstract

A stochastic multi-cloud model (SMCM) convective parameterization is incorporated in the National Centers for Environmental Predictions' Climate Forecast System version 2 (CFSV2). The resulting model is referred to here as CFSsmcm. Two 15 year long climate simulations of the CFSsmcm, differing only by one SMCM parameter, namely, the mid-tropospheric dryness parameter, MTD0, are analyzed and interpreted here. This particular parameter is chosen because not only it plays a crucial role in the SMCM formulation, but also is observed to be critical for triggering tropical convection. In one case we have used a single homogeneous MTD0 value for the entire globe and in the other run two different MTD0 values are used for land and ocean. The global precipitation climatology significantly improves in the inhomogeneous MTD0 case without significantly affecting the excellent performance of the CFSsmcm in terms of the intra-seasonal and synoptic variability as documented in previous publications.

1 Introduction

The importance of the role played by a convective parameterization (CP) scheme can never be overemphasized in a global climate model (GCM). Most of the biases in a simulated climate originate from the inaccuracy in representing the subgrid scale convective elements [*Randall*, 2013; *Arakawa*, 2004]. Quest for an efficient CP scheme has been on for a few decades now [*Kuo*, 1965; *Arakawa and Schubert*, 1974; *Betts and Miller*, 1986; *Kain and Fritsch*, 1990; *Gregory and Rowntree*, 1990; *Zhang and McFarlane*, 1995]. The assumptions these CP schemes are based on, stem from our understanding of atmospheric convection. However, there is one feature common to all these different schemes: they are all deterministic in nature. Or in other words, these schemes do not account for the sub-grid scale variability among the different convective elements. The basis for a deterministic convective parameterization is the underlying assumption that, a typical GCM grid size is large enough to encompass a large ensemble of the clouds, which are in quasi-equilibrium with the large scales and that the large-scale mean ensemble is uniquely determined [*Arakawa and Schubert*, 1974]. However, with the increasing resolution of the present day GCMs, the validity of this assumption needs to be reevaluated [*Palmer*, 1996]. Consequently, there is an undeniable possibility that neglecting the variability of the subgrid scale convective elements may lead to biases in the mean climate [*Palmer*, 2001]. Efforts to adequately represent these convective systems in a GCMs has led the scientific community to think beyond conventional CP schemes. Superparamaterized GCMs (SP-GCM) [*Grabowski*, 2001; *Khairoutdinov and Randall*, 2001] and global cloud resolving models (GCRM) [*Satoh et al.*, 2005] (also see *Randall* [2013] for a review) are such promising approaches. However, SP-GCMs and GCRMs are computationally expensive and definitely unlikely candidates for operational centers; especially for ensemble predictions. Nevertheless, the success of these approaches highlighted the importance of accurate representation of the sub-grid scale (SGS) variability collectively while realizing the individual behaviour of the convective elements, in the GCMs and their impact on the large-resolved scales. In the spirit of superparameterization, a computationally significantly less expensive approach was introduced in *Khouider et al.* [2010]; the authors termed it as the stochastic multi-cloud model convective parameterization. This was the descendant of the same multi-cloud model introduced in *Khouider and Majda* [2006] but with the added feature of stochasticity.

Driven by the general consensus that a faithful representation in some way of the sub-grid scale convective variability is probably the only way forward, stochastic approaches to the convective parameterization problem are getting more attention in the recent times than ever before [*Buizza et al.*, 1999; *Lin and Neelin*, 2000, 2002, 2003; *Palmer*, 2001; *Majda and Khouider*, 2002; *Khouider et al.*, 2003; *Plant and Craig*, 2008; *Teixeira and Reynolds*, 2008; *Deng et al.*, 2015, 2016; *Ajayamohan et al.*, 2016; *Davini et al.*, 2016]. In order to introduce stochasticity to an existing deterministic convective parameterization, different methods have been adopted. The perturbed parameterization tendencies approach introduced by *Buizza et al.* [1999] consists of multiplying the CP outputs by correlated or non-correlated random numbers at each GCM column [*Davini et al.*, 2016, and references therein]. *Teixeira and Reynolds* [2008] followed a similar technique as *Buizza et al.* [1999] but they multiplied only the convective tendencies. *Lin and Neelin* [2000] added stochasticity to a deterministic scheme by adding a zero-mean red noise to the its closure equation, namely the convectively available potential energy (CAPE) closure equation. In the study by *Lin and Neelin* [2002], a distribution of precipitation is assumed a priori to control the statistics of the overall convective heating. *Lin and Neelin* [2003] tested a stochastic deep convective parameterization in a general circulation model for the first time. *Plant and Craig* [2008] used equilibrium statistical mechanics to derive a Poisson distribution for convective plumes based on radiative convective equilibrium cloud resolving simulations. *Majda and Khouider* [2002] and *Khouider et al.* [2003] used a Markov process on a lattice for convective inhibition. The stochastic lattice approach has been extended in *Khouider et al.* [2010] to derive the stochastic multicloud model (SMCM), designed to mimic the interactions at sub-grid scales of multiple cloud types in the tropics. The SMCM has been extensively used and evaluated in simple models for organized convection and convectively coupled equatorial waves (CCEW) [*Frenkel et al.*, 2012, 2013; *Peters et al.*, 2013; *De La Chevrotière et al.*, 2015; *De La Chevrotière and Khouider*, 2017]. Moreover, the SMCM has been successfully adopted as a cumulus parameterization in an aquaplanet GCM to simulate the Madden-Julian oscillation (MJO), CCEWs and Indian summer monsoon intra-seasonal oscillations (MISOs) [*Deng et al.*, 2015, 2016; *Ajayamohan et al.*, 2016]. In this chapter, we present the highlights of the simulated climate when the SMCM, is incorporated into the National Centers for Environmental Prediction (NCEP) Climate Forecast System version 2 (CFSv2) model (referred to as CFSsmcm hereafter) in lieu of the pre-existing simplified Arakawa-Schubert (SAS) cumulus scheme.

A first insight into the CFSsmcm simulated climate is provided in *Goswami et al.* [2017a]. They demonstrated that while retaining an equally good mean state (if not better) as the parent model (CFSv2), CFSsmcm significantly improved the synoptic and intra-seasonal variability; provided a better account of convectively coupled equatorial waves and the Madden-Julian oscillation (MJO); exhibited better northward and eastward propagation of intra-seasonal oscillation of convection including the MJO propagation beyond the maritime continent barrier. The distribution of precipitation events was also found to be better simulated in CFSsmcm which was severely biased towards too much drizzling precipitation in the parent model. An overview of the SMCM formulation, and the development and tuning of the CFSsmcm in detail can be found in *Goswami et al.* [2017b], where the model's sensitivity to the key parameters of the SMCM formulation is reported through a comparative analysis of a few 5-year long climate simulations in order to distinguish the best possible set of SMCM parameters for the CFSsmcm model. The model was found to be most sensitive to the mid-tropospheric dryness parameter (MTD) and to the stratiform cloud decay timescale (τ_{30}). MTD was more effective in controlling the global mean precipitation and its distribution while τ_{30} had more effect on the organization of convection as noticed in the simulation of the Madden-Julian oscillation (MJO). This is consistent with the fact that, in the SMCM formulation, mid-tropospheric humidity controls the deepening of convection and stratiform clouds control the backward tilt of tropospheric heating and the strength of unsaturated downdrafts which cool and dry the boundary layer and trigger the propagation of organized convection [*Ajayamohan et al.*, 2016; *Deng et al.*, 2016]. Noteworthy, the CFSsmcm model was found to be robust in the sense that the simulated mean climate appeared resilient to small changes in the parameter values. A detailed analysis of the tropical intra-seasonal variability (TISV) and convectively coupled equatorial waves (CCEW), in comparison with the parent GCM and with observations, was presented in *Goswami et al.* [2017c]. Significant improvements were noted in the simulation of the Madden-Julian oscillation (MJO) and most of the CCEWs as well as the Indian summer monsoon (ISM) intra-seasonal oscillation (MISO). The authors also demonstrated these improvements to be a result of improved mechanisms and physical structure of these oscillations. They also found that, improved representation of interaction of the multiple clouds in the SMCM formulation holds the basis of this improved climate simulation by the CFSsmcm model. The SMCM has been used to modify the triggering of deep convection in the German GCM ECHAM4 and noticeable improvements are seen, especially in terms of the ability of the model to represent tropical rainfall variability [*Peters et al.*, 2017]. A variant of the SMCM has also been adopted and used to stochastisize an existing CP in *Dorrestijn et al.* [2016].

Upon the implementation CFSsmcm, an extensive parameter testing has been conducted by making several short 5-year runs. A few of these simulations codified with whole numbers, are reported in *Goswami et al.* [2017b] providing a first hand analysis of the model's parameter sensitivity and behavior. In this chapter we take Run 139 from Table 1 of *Goswami et al.* [2017b] and run it to simulate a 15-year long climate and then compare the results with that of Run 129. It should be noted that Run 129 is the only CFSsmcm run which has been extensively analyzed and reported in detail in *Goswami et al.* [2017a] and *Goswami et al.* [2017c]. The Run 129 was selected from a number of 5-year long simulations based on a few basic metrics reported in *Goswami et al.* [2017b]. Some changes, more often good, in the simulated mean state and variability were noted when we ran Run 129 for 15 years. In *Goswami et al.* [2017b], the closest competitor to Run 129 was Run 139. The only difference between the two runs resides in the way the mid-tropospheric dryness parameter, MTD0, is prescribed. The physical significance of MTD0 is that, it decides how moist the middle atmosphere needs to be to initiate convection. In the SMCM formulation, a small MTD0 means that the middle troposphere needs to be very moist to allow deep convection. From *Goswami et al.* [2017b], we recall that Run 129 uses a single uniform value of MTD0 $= 5$, for the entire globe, while in Run 139 we have set that, MTD0 $= 5$ over the oceans and MTD0 $= 25$ over the continents. In other words, in Run 139, the atmosphere over the oceans wait longer to initiate convection than it does over continents. However, one MTD0 value for the entire globe implies no such distinction in Run 129. *Goswami et al.* [2017b]

briefly discussed the benefits of using distinct MTD0 values, one over land and one over the oceans, over using a single MTD0 value for the entire globe. A few crucial improvements were achieved with the variable-MTD0 runs including the precipitation climatology. In particular, the dry bias in the simulated Indian summer monsoon rainfall was significantly reduced. As a consequence, the poleward migrations of convection bands over the Indian monsoon region also had improved while the Takayabu-wheeler-Kiladis (TWK) spectra [*Takayabu*, 1994; *Wheeler and Kiladis*, 1999] remained almost unchanged. They explained this improvement by the fact that, the variable MTD0 affects primarily the mean while the intraseasonal and synoptic variability are mostly affected by convection over the oceans.

The motivation behind this exercise is not to find out the better one between Run 129 and 139. Rather, we want to highlight the possibilities offered by the CFSsmcm model as a virtual laboratory to study the interaction between convection and cloud and the climate system. More than summarizing the results in a review mode, we wish to explore the scopes and opportunities of SMCM. Comparing the runs 129 and 139, which differ only by one parameter value, may seem like just a simple tuning exercise, but because of the role played by that particular parameter, MTD0 (the scaling value for the middle tropospheric dryness), in the SMCM formulation we expect to get valuable guidance towards improving the SMCM formulation further.

The rest of this chapter is organized as follows: the SMCM framework, including the developmental and implementation aspects, is explained in the section 2. Section 3 presents and compares the numerical results obtained with the two MTD0 configurations. Finally a concluding discussion is provided in the 4th section.

2 The SMCM formulation

2.1 Parameterization of the Total Heating

The stochastic multicloud model uses 3 prescribed profiles for convective heating, ϕ_c, ϕ_d and ϕ_s, associated with cumulus congestus cloud decks (which warm and moisten the lower troposphere and cool the upper troposphere through radiation and detrainment), deep cumulonimbus clouds (which heat up the whole atmospheric column) and stratiform cloud types lagging deep convection (which heat the upper troposphere and cool the lower troposphere due to the evaporation of stratiform rain), respectively.

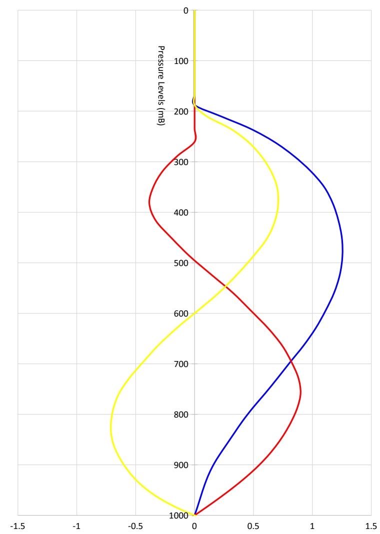

Figure 1. Basis Functions. Cumulus congestus profile in Red; Deep Cumulus profile in Blue; and Stratiform profile in Yellow.

While in the original multicloud-model [*Khouider and Majda*, 2006, 2008], simple sine functions were used to set up the basis functions and *Khouider et al.* [2011] used the vertical mode eigenstructure of *Kasahara and Puri* [1981] the CFSsmcm implementation combines observational studies with theory on tropical heating profiles to construct ϕ_c, ϕ_d, ϕ_s. The shape of the deep heating basis function is designed based on the average heating profile in Fig-3 of *Stachnik et al.* [2013]. The stratiform basis function is designed following the Stratiform heating profile reported in Fig-1 of *Schumacher et al.* [2007]. The congestus heating profile is designed following *Khouider and Majda* [2006], but slightly modified to represent the lower level peak (around 700hPa) noted in the convective heating profiles plotted from the CFSR data (not shown here). When constructing ϕ_c, we have also consulted the work of *Schumacher et al.* [2007] (The "Shallow convective" and the "Strongly detraining Cu congestus" profiles in their Fig-1). Incidentally (as it can be seen in Fig-1), the heating basis functions were clipped to zero at or slightly below 200 hPa. This is somewhat arbitrary as there are instances where the tropaupose level is higher and it is not clear how much the results would change if this level was a bit higher or lower. This will be the subject of future studies.

The total convective heating is:

$$Q_{tot}(z) = H_d \phi_d(z) + H_c \phi_c(z) + H_s \phi_s(z). \tag{1}$$

Here, ϕ_c, ϕ_d and ϕ_s are the three basis functions shown in Figure 1; and H_c, H_d and H_s are the associated heating rates, which are parameterized using the corresponding stochastic area fractions, σ_d, σ_c and σ_s respectively, and the large-scale dynamical variables:

$$H_d = \frac{\sigma_d}{\bar{\sigma}_d} Q_d, \tag{2}$$

$$H_c = \frac{\sigma_c}{\bar{\sigma}_c} \alpha_c Q_c, \tag{3}$$

$$\frac{\partial H_s}{\partial t} = \frac{1}{\tau_s} \left[\frac{\sigma_s}{\bar{\sigma}_s} \alpha_s H_d - H_s \right]. \tag{4}$$

Here, $\bar{\sigma}_c$, $\bar{\sigma}_d$ and $\bar{\sigma}_s$ are the background values of σ_c, σ_d and σ_s, respectively, α_c and α_s are the congestus and stratiform adjustment coefficients, respectively, and τ_s is the stratiform convection adjustment time-scale.

According to *Khouider et al.* [2010] the cloud area fractions σ_c, σ_d and σ_s describe a Markov jump stochastic process in the form of a multi-dimensional birth-death process whose transition probabilities depend explicitly on the mid tropospheric dryness (MTD), convective available potential energy (CAPE) and convective inhibition (CIN) and vertical velocity (W). The formulation of the transition rates from one cloud type to the other are the same as prescribed in *Deng et al.* [2015], except for the formation of congestus and deep convection from clear sky condition. This change occurs due to the inclusion of CIN and W in the transition rules. The inclusion of CIN and W in the transition rates are driven the desire to make the deep convection paramaterization aware of the shallow convection scheme in the sense that in the event of strong subsidence and/or strong CIN, deep convection is inhibited leaving "space" for shallow convection which is naturally promoted in such circumstances. The modified transition rates (formation rates of congestus and deep clouds are highlighted in bold) are given in Table 1. The values of the transition time scales, on the last column of Table 1, are from *De La Chevrotière et al.* [2015], who used a systematic Bayesian inference technique to learn these parameters from large eddy simulation data [*Khairoutdinov et al.*, 2009].

In Eqn (2-4), the potentials for deep (Q_d) and congestus (Q_c) convection are computed, using the following equations,

Table 1. SMCM transition rules. The transition rates are given in terms of the large scale predictors CAPE, $C = CAPE/CAPE0$, Low level CAPE, $C_L = LCAPE/LCAPE0$, dryness, $D = \mathcal{H}/MTD0$, where $\mathcal{H}$ is the relative humidity, large scale subsidence, $W_N = -\min(0, W/W0)$, and $C_N = -CIN/CIN0$. Here $LCAPE$ is the part of the CAPE integral between LFC and the freezing level. We note that CIN is by definition a negative definite quantity, so that when CIN is large, $\Gamma(C_N) \longrightarrow 1$.

Description	Transition Rate, where $\Gamma(x) = \begin{cases} (1-e^{-x}), & \text{if } x > 0 \\ 0, & \text{otherwise} \end{cases}$	Time Scale (hours)
Formation of congestus	$R_{01} = \frac{1}{\tau_{01}}(\Gamma(C_L)\Gamma(D)^{\frac{\mathbf{(1-\Gamma(W_N))+(1-\Gamma(C_N))}}{\mathbf{2}}}$	τ_{01}=32
Decay of congestus	$R_{10} = \frac{1}{\tau_{10}}\Gamma(D)$	τ_{10}=2
Conversion of congestus to deep	$R_{12} = \frac{1}{\tau_{12}}\Gamma(C)(1-\Gamma(D))$	τ_{12}=0.25
Formation of deep	$R_{02} = \frac{1}{\tau_{02}}(\Gamma(C)(1-\Gamma(D))^{\frac{\mathbf{(1-\Gamma(W_N))+(1-\Gamma(C_N))}}{\mathbf{2}}}$	τ_{02}=12
Conversion of deep to stratiform	$R_{23} = \frac{1}{\tau_{23}}$	τ_{23}=0.25
Decay of deep	$R_{20} = \frac{1}{\tau_{20}}(1-\Gamma(C))$	τ_{20}=9.5
Decay of stratiform	$R_{30} = \frac{1}{\tau_{30}}$	τ_{30}=1

$$Q_d = \left[\bar{Q_d} + \frac{1}{\tau_q}\frac{L_v}{C_p}q_m^{'} + \frac{1}{\tau_c}\left(\theta_{eb}^{'} - \gamma_c\theta_m^{'}\right)\right]^+, \tag{5}$$

$$Q_c = \left[\bar{Q_c} + \frac{1}{\tau_c}\left(\theta_{eb}^{'} - \gamma_c\theta_m^{'}\right)\right]^+. \tag{6}$$

In the equations (5) and (6), $\bar{Q_d}$, $\bar{Q_c}$, $\bar{Q_s}$ are prescribed background potentials for deep, congestus and stratiform convection respectively. They are inferred from CFS reanalysis data [*Saha et al.*, 2010] by projecting the climatological convective heating, Q_1 onto the three basis functions in (1). The parameters τ_q and τ_c are the convective adjustment time scales of moisture and temperature, respectively. The quantities $q_m^{'}$, $\theta_{eb}^{'}$, $\theta_m^{'}$ are given by,

$$q_m^{'} = q_m - \bar{q_m} \tag{7}$$

$$\theta_{eb}^{'} = \theta_{eb} - \bar{\theta_{eb}} \tag{8}$$

$$\theta_m^{'} = \theta_m - \bar{\theta_m}. \tag{9}$$

They are the deviations of the model's middle troposphere moisture, equivalent potential temperature, in the planetary boundary layer (PBL) and middle troposphere potential temperature, respectively, from their background states denoted by over bars. These background values are set according to the climatology of 20 year CFSR data averaged in space over distinct regional boxes in Figure 2.

Earlier theoretical studies with the SMCM [*Khouider and Majda*, 2006; *Khouider et al.*, 2010; *Deng et al.*, 2015, and the relevant references therein] all rely on the radiative convective equilibrium (RCE) solution (space-time homogeneous solution) of the governing equations to construct the background to set up the parameterization in Equations (2) to (10). However, such solution is not practical in the context of a comprehensive climate model because of existence of various inhomogeneities, like, land-ocean, tropics-mid latitude, etc. To overcome this conundrum we have used climate data to compute surrogates for the RCE solution as time and spatial means for a set of boxes centered over different areas of relatively homogeneous climatologies. These different areas (boxes) of relatively homogeneous climatologies are shown in Figure 2 overlaid over the shows the long term mean of specific humidity at the surface, which provide a rationale behind choosing these boxes. We have plotted other thermo-dynamical fields as well (not shown here), before deciding on the partition boxes. Noteworthy, we have smoothed each background fields before prior to the implementation into CFSsmcm. As an example of a background field, the middle level specific humidity is shown in Figure 3.

Furthermore, the CFSsmcm includes an unsaturated downdraft mass flux which serves to cool and dry the lower troposphere due to the evaporation of stratiform rain in the lower troposphere. It is given by,

$$D_c = \mu \left[\frac{H_s - H_c}{\bar{Q}_c} \right]^+, \tag{10}$$

where, $\mu = 1.25cms^{-1}$ is the downdraft reference scale. Here and elsewhere in the paper X^+ denotes the positive part of the variable X, i.e., $\max(X, 0)$.

In the equations in (5) and (6), the subscript b indicates variables averaged over the boundary layer height defined as, $X_b = \frac{1}{h} \int_0^h X(z)\, dz$. The PBL height, h, is inputted from CFSv2. The height of the stable PBL, h, is estimated iteratively from ground up using bulk Richardson number (R_b) until a critical value $R_{bc} = 0.25$ is reached [*Troen and Mahrt*, 1986]. Incidentally, h is the height of the mixed layer which is consistent with the design of the multicloud model [*Khouider and Majda*, 2006, 2008; *Waite and Khouider*, 2009]. The subscript m indicates values of the variables taken at the middle troposphere. The middle level specific humidity is chosen at 700 hPa. This is based on the long term mean (obtained from CFSR 20 year reanalysis data) of moist static energy (MSE) profile. We have chosen the level where a minimum in the MSE profiles is noted (for those boxes which lie within 40S-40N in Fig-2). Based on the climatological profiles of equivalent potential temperature (θ_e) and convective heating (not shown here), we have defined the middle and low troposphere value of θ_e at 500hPa and 700hPa, respectively.

2.2 Prescribed vertical profiles of moistening and drying

The moisture sink is set to:

$$P(z) = -\frac{c_p}{L_v} \langle Q_{tot} \rangle Q_2(z), \tag{11}$$

where $\langle Q_{tot} \rangle$ is the vertical average of the total heating $Q_{tot}(z)$, c_p is the specific heat at constant pressure, L_v is the latent heat of vaporization, and $H = 16$ km is the a rough estimate of the tropospheric height. Moreover, $Q_2(z)$ is a prescribed moisture sink function whose exact shape is given in Figure 4 and its vertical average is unity.

The surface precipitation is given by

$$P = \frac{c_p}{L_v} \int_0^H Q_{tot}(z) dz. \tag{12}$$

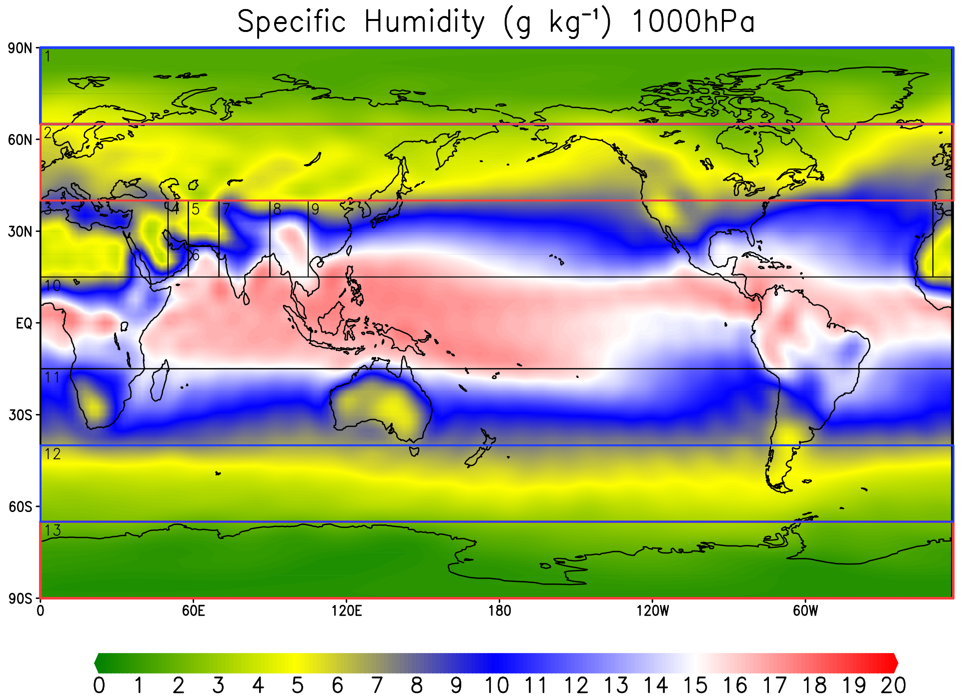

Figure 2. Long term mean of specific humidity at the surface (computed from Climate Forecast System Reanalyses product).

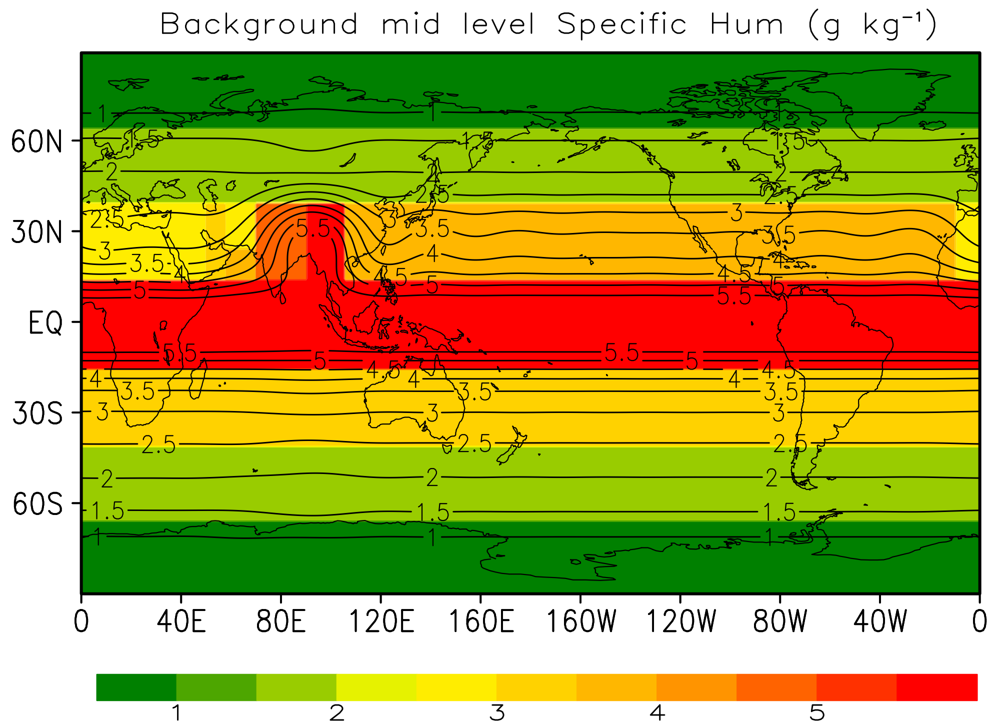

Figure 3. Background mid level (700 hPa) Specific Humidity (g/kg). In shading is the non-smoothed box-wise values. Smoothed field for the same is shown by the overlaid contours.

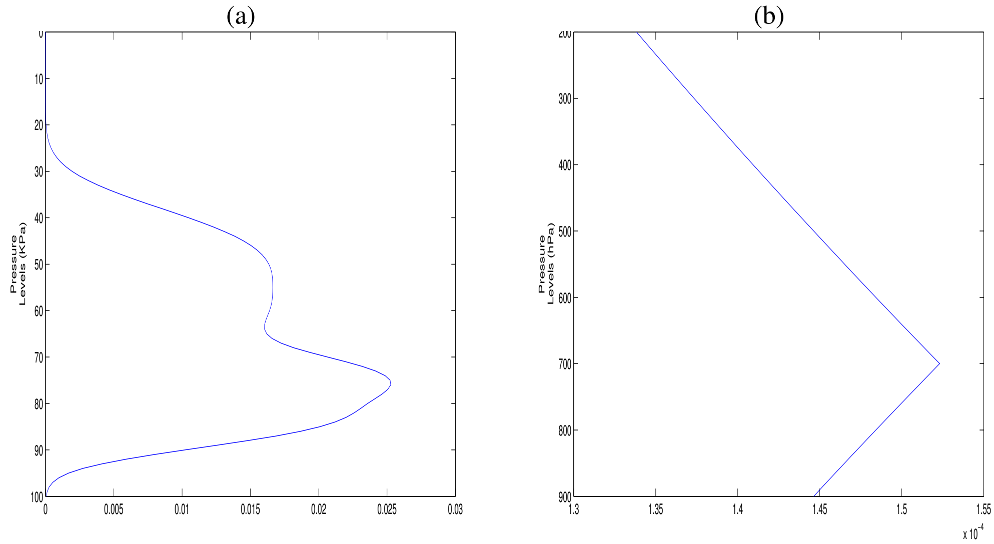

Figure 4. (a) The shape of the $Q_2(z)$ structure function in the moisture sink eq. 11 (drying). (b) The shape of the $\delta_m(z)$ structure function in eq. 13 (moistening).

The introduction of the structure function $Q_2(z)$ is a new feature of this current version of SMCM. The shape of $Q_2(z)$ (Figure 4a) is inspired by the Yanai moisture sink profile [*Yanai et al.*, 1973]. In earlier versions of the SMCM, the moisture sink is set according to the fact that only the column integrated water vapor is integrated, i.e, the free tropospheric moisture is represented by one single vertical grid point. In this context, under the constraint of the conservation of vertically integrated moist static energy, the precipitation rate reduces to the vertical integral of the convective heating potential temperature tendency, renormalized by the ratio of the latent heat of vaporization and the specific heat at constant pressure. The moisture sink closure provided in Eq 11 was derived under the same constraint of moist static energy conservation.

The evaporation rate is given by,

$$E(z) = \left(\delta_m(z)\frac{D_c}{H}\right)\triangle_m\theta_e, \tag{13}$$

where, $\triangle_m X = X_b - X_m$, with the suffixes b and m indicating respectively the PBL and middle troposphere values of the variable X. The structure function $\delta_m(z)$ (Figure 4b) is defined by:

$$\delta_m(z) = \begin{cases} 2\exp\left(-\alpha_m\frac{|P(z)-P_{MID}|}{P_{BOT}-P_{TOP}}\right), & \text{if } z \geq h \\ 0, & \text{if } z < h \end{cases} \tag{14}$$

where α_m is a constant, so that, $\frac{1}{H}\int_0^H \delta_m(z) = 1$

The expression $P(z) = -\frac{c_p}{L_v}\langle Q_{tot}\rangle Q_2(z)$ ensures that the vertically averaged convective heating balances the total amount of precipitation reaching the ground while that of the evaporation rate, $E(z)$, is designed to balance the drying and cooling of the PBL by downdrafts so that the vertically averaged moist static energy is conserved as anticipated.

The SMCM feeds back onto the dynamical core variables through the temperature and moisture convective tendencies given by,

$$\left[\frac{\partial}{\partial t}\theta(z)\right]_{SMCM} = Q_{tot}(z) - D_{b\theta} \tag{15}$$

$$\left[\frac{\partial}{\partial t}q(z)\right]_{SMCM} = -P(z) + E(Z) - D_{bq} \tag{16}$$

Here, $D_{b\theta}$ and D_{bq} represent the effect of unsaturated downdraft which result in cooling and drying below the PBL (h, which is a variable imported from the CFSv2 boundary layer scheme into the SMCM module), and they are given by

$$D_{bq}(z) = \begin{cases} \frac{D_c}{h}\triangle_m q & \text{if } z < h, \text{ results drying,} \\ 0 & \text{if } z > h, \end{cases} \tag{17}$$

$$D_{b\theta}(z) = \begin{cases} \frac{D_c}{h}\triangle_m \theta & \text{if } z < h, \text{ results cooling,} \\ 0 & \text{if } z > h. \end{cases} \tag{18}$$

While the GCM dynamical core has time step of 10 minutes, the SMCM convective tendencies in Eqns. (13) and (14) are updated every 10 seconds, i.e., 60 times per GCM time step in order to ensure stability, due to the fast convective timescale.

A comprehensive list of parameters that appear in the equations (1)-(18) and their values are provided in Table 3. The first column of Table 3 refers to the number of the equation where the parameters appear for first.

3 Results

In this section we compare two longtime simulations corresponding to runs 129 and 139 from *Goswami et al.* [2017b], by comparing their mean state and their intra-seasonal variability against observational benchmarks consisting of TRMM rainfall [*Huffman et al.*, 2010] and NCEP reanalysis data [*Kalnay et al.*, 1996] for temperature, moisture and wind fields.The CFSsmcm simulations are based on a T126 horizontal resolution combined with 64 vertical levels and a 10 minute time step. The SMCM birth-death process is simulated via Gillespie's exact Monte-Carlo algorithm, which is run in parallel at every GCM time step

Table 2. List of parameters

Reference	Parameter	Value	Remarks
3	α_c	0.1	Congestus adjustment coefficient
4	τ_s	96 hrs	Stratiform convection adjustment timescale
4	α_s	0.2	Stratiform adjustment coefficient
5	τ_q	144 hrs	Moisture adjustment timescale
5	L_v	$2.5 \mathrm{x} 10^6$ J kg^{-1}	Latent heat of condensation
5	C_p	1004.6 J kg^{-1} K^{-1}	Specific heat of air at constant pressure
5	τ_c	240 hrs	Congestus convection adjustment timescale
5	γ_c	0.1	Adjustment coeff. for relative contribution of congestus to deep heating
10	μ	1.25 cm s^{-1}	Downdraft reference scale
12	H	16km	Height of the tropical troposphere
14	α_m	0.22	—

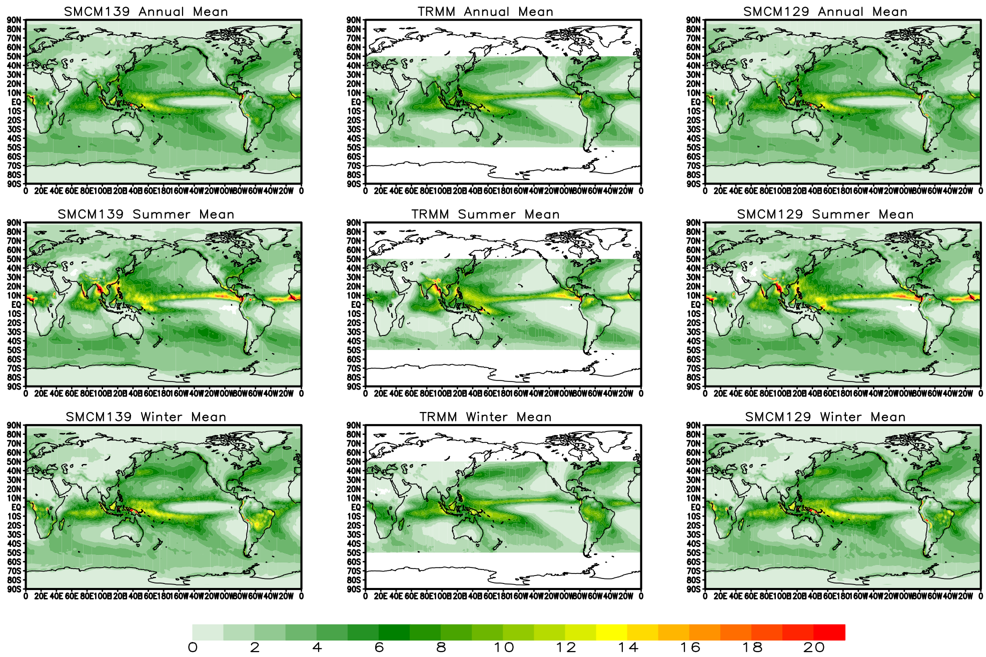

Figure 5. Annual and seasonal (summer: JJAS and winter:O-M) mean rainfall fields (mm day^{-1}) for Run 139 (left hand side panels), TRMM (middle panels) and Run 129 (right hand side panels).

(see *Khouider et al.* [2010], for details). As mentioned earlier the key difference between the two SMCM simulations presented here resides in the way the mid-troposphere dryness parameter, MTD0, appearing in the caption of Table 1, is set. Run 129 uses a single value of MTD0=5 globally while Run 139 uses two values simultaneously, by setting MTD0=25 over land and MTD0=5 over the ocean.

3.1 Mean state

The simulated precipitation fields are shown in Figure 5, where the annual mean and the summer and winter seasonal means are displayed separately. It is evident from the annual mean, and individually for the two seasons as well, the precipitation field has significantly improved in Run 139. The wet bias over the oceans and the dry bias over the continents have significantly reduced. Overall, the geographical distribution of the precipitation looks much better in Run 139. Improvement in the simulation of the Indian summer monsoon mean state is one of the major gains of Run 139 over Run 129. As a more convincing evidence, we have plotted the climatological annual cycle of rainfall over the Indian summer monsoon domain in Figure 6. We consider three different boxes over the ISM domain and plotted the climatological annual cycle of rainfall over each box. Clearly, Run 139 simulation matches the

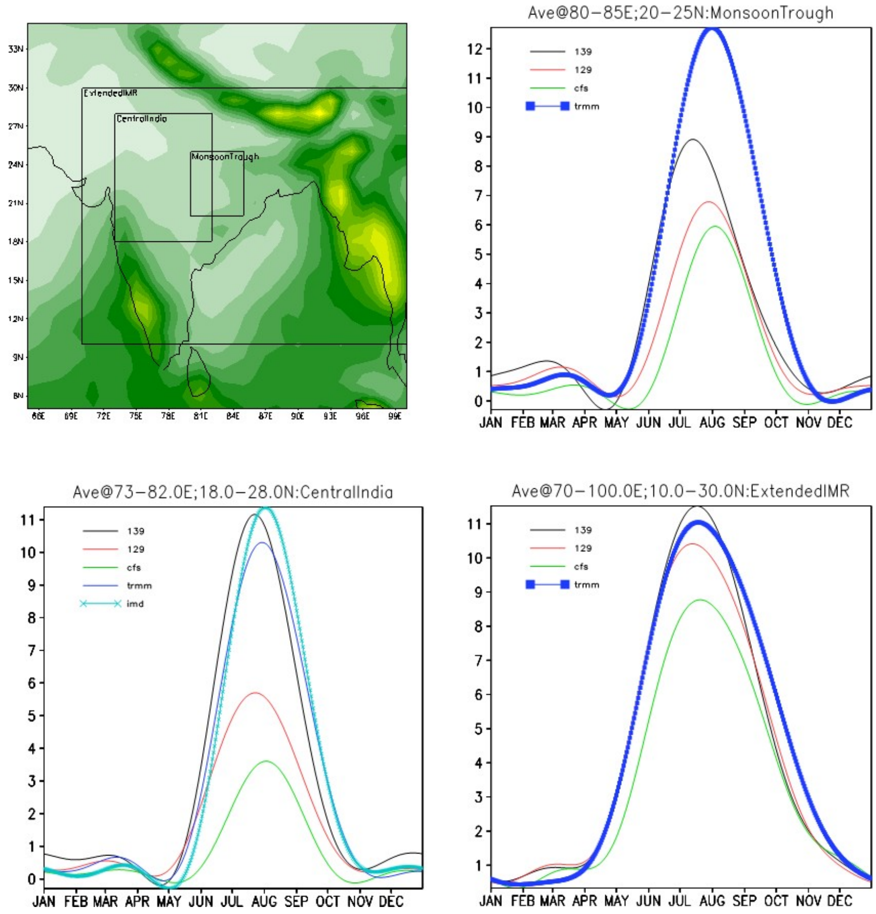

Figure 6. Annual cycle of climatological daily mean rainfall (mm day^{-1}) over the Indian monsoon region (different boxes).

observation fairly well and much better than Run 129 and the CFSv2 control run. For both the boxes "Central India" and "Extended IMR", Run 139 looks consistent with observation. Importantly, the improved annual cycle is actually due to good distribution of rainfall and not due to any compensation of rainfall covering the dry bias over India by wet bias over the mountainous terrains. However, Run 139 still looks dry over the box "Monsoon trough" accompanied by an early withdrawal.

3.2 Intra-seasonal Variability

Capturing the intra-seasonal variability has been a key achievement of the SMCM effort in its idealized simulations [*Deng et al.*, 2015, 2016; *Ajayamohan et al.*, 2016] as well as when implemented in CFS [*Goswami et al.*, 2017a,c]. Another feature of the CFSsmcm has been its resilience in terms of minor changes to its parameter values [*Goswami et al.*,

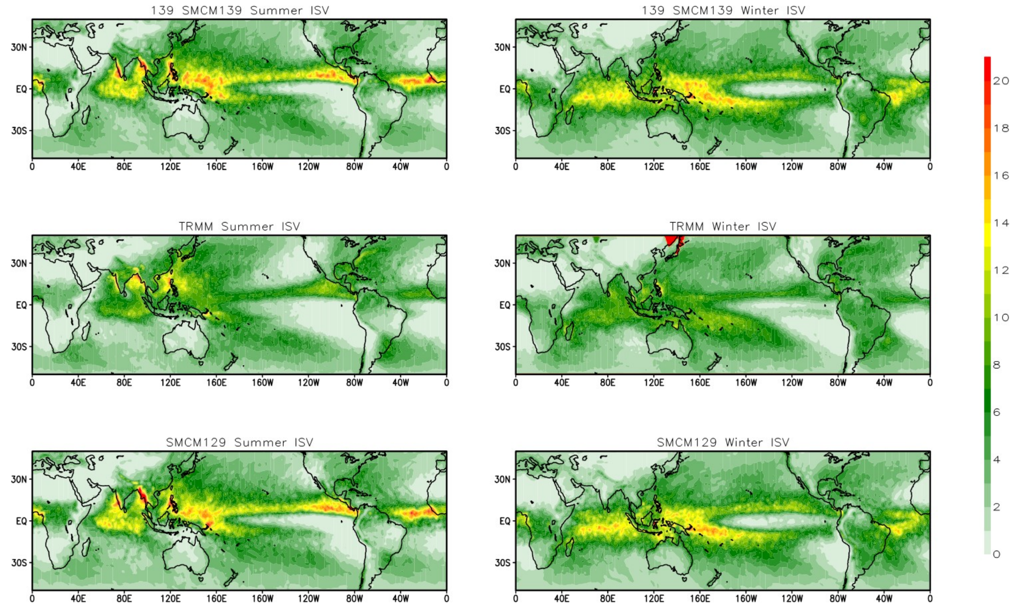

Figure 7. Intra-seasonal variability (standard deviation of the 10-90 day bandpass filtered rainfall anomalies) for Run 139 (top panels), TRMM (middle panels) and Run 129 (bottom panels), for the summer and winter seasons.

2017b]. Since changing the value of the middle tropospheric dryness parameter is a considerable change from SMCM's perspective, we examined the response of the CFSsmcm Run 139 in capturing the intra-seasonal variability. In Figure 7, we have plotted the standard deviation of 10-90 day bandpass Lanczos filtered rainfall anomalies for the two seasons. This gives an overview of the intra-seasonal variability in the simulated precipitation fields. Comparing the runs 129 and 139, the intra-seasonal variability does not change significantly. As we have already mentioned, resilience to changes in parameter values has been a hallmark of the CFSsmcm throughout its development [*Goswami et al.*, 2017b]. Nevertheless, there are slight increases in variability observed over the Western Pacific and the Indian landmass. This increase in variability is consistent with the increase in the mean seasonal rainfall.

3.3 Tropical wave spectrum

When implementing the SMCM in CFSv2, the simulation of the tropical intra-seasonal variability (TISV) improved significantly compared to the default CFSv2 simulation, evident from the Takayabu-Wheeler-Kiladis (TWK) diagram [*Goswami et al.*, 2017c]. Therefore we plotted the same for Run 139 to see if the improvements are retained or changed. In Figure 8

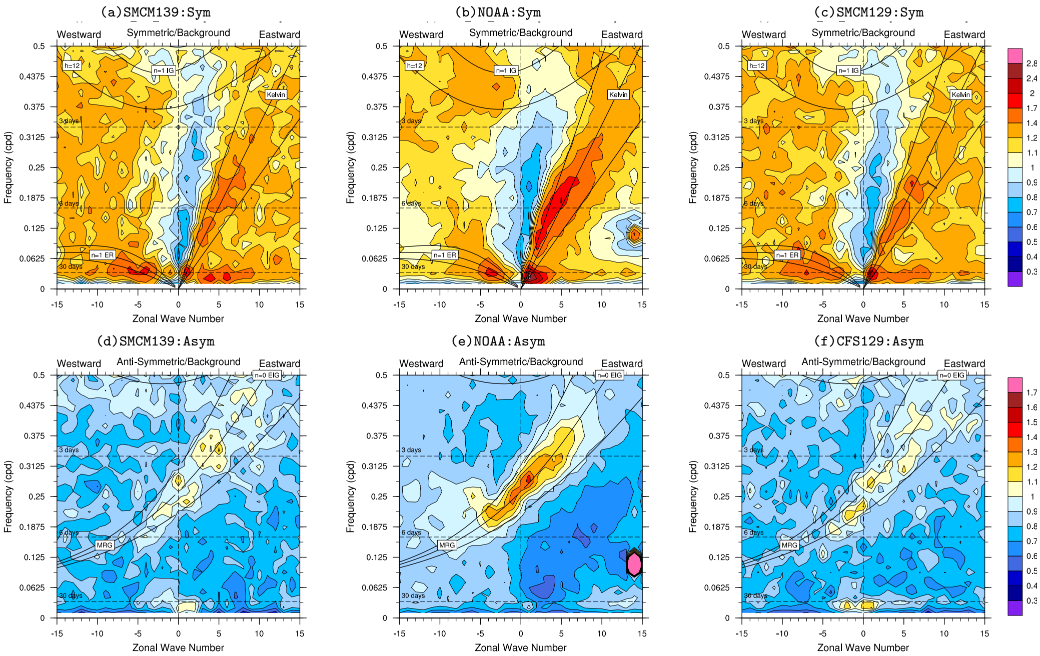

Figure 8. Wheeler-Kiladis spectra of OLR from (a)Run 139, (b)NOAA OLR and (c) Run 129, for the symmetric component. The corresponding anti-symmetric spectra are shown in panels d, e and f, respectively.

the TWK diagram for the outgoing long-wave radiation (OLR) is shown for the whole length of the 10-year climate for the runs 129 and 139 and observation (OLR from the National Oceanic and Atmospheric Administration; *Liebmann and Smith* [1996]). As evident from the faded color shading, Run 139 is relatively less skillful compared to Run 129. However, Run 139 still outperforms the control CFSv2 run (See Figure 1b and 1c of *Goswami et al.* [2017c]). Except the equatorial Rossby waves, there is a loss power in all other modes of the tropical wave spectrum. Especially the MJO mode appears somewhat weak with unrealistic power in higher wave-number regime.

3.4 MJO variability and propagation

The MJO is the major mode of variability in the tropics on the intra-seasonal timescales. Also, it is notoriously difficult to simulate realistically by coarse resolution climate models. Hence it can be treated as a metric for the fidelity of a climate model in simulating the tropical variability at such scales. *Goswami et al.* [2017c] showed that CFSsmcm simulates the MJO significantly better compared to the default CFSv2 model. Now, as we have already seen in the previous subsection 3.2, that the TWK plot has slightly deteriorated in Run 139,

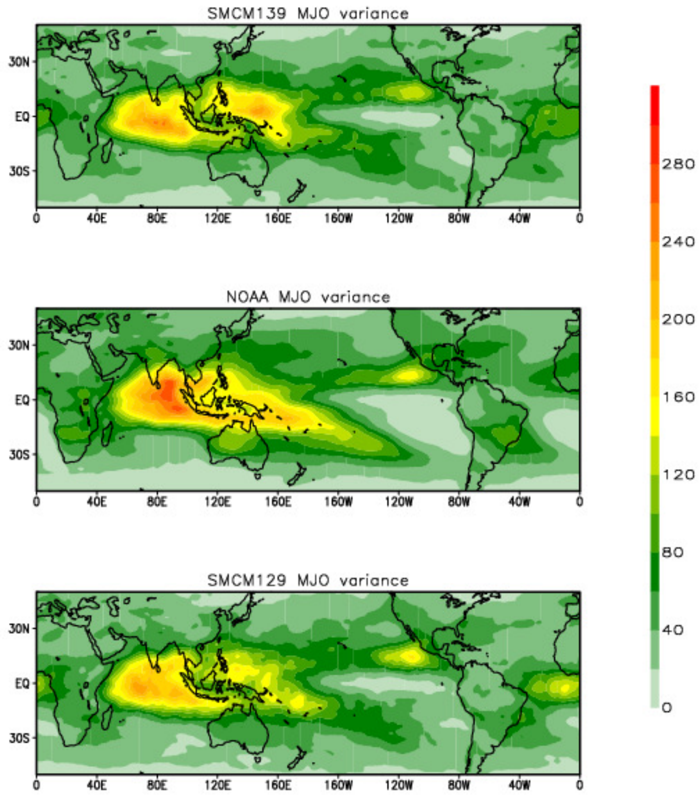

350 **Figure 9.** Daily variance of the MJO filtered (wavenumber 1-9 and 36-90 days) OLR ((W $m^{-2})^2$) anomalies: Run 139 (top), OBS (NOAA OLR) (middle) and Run 129 (bottom).

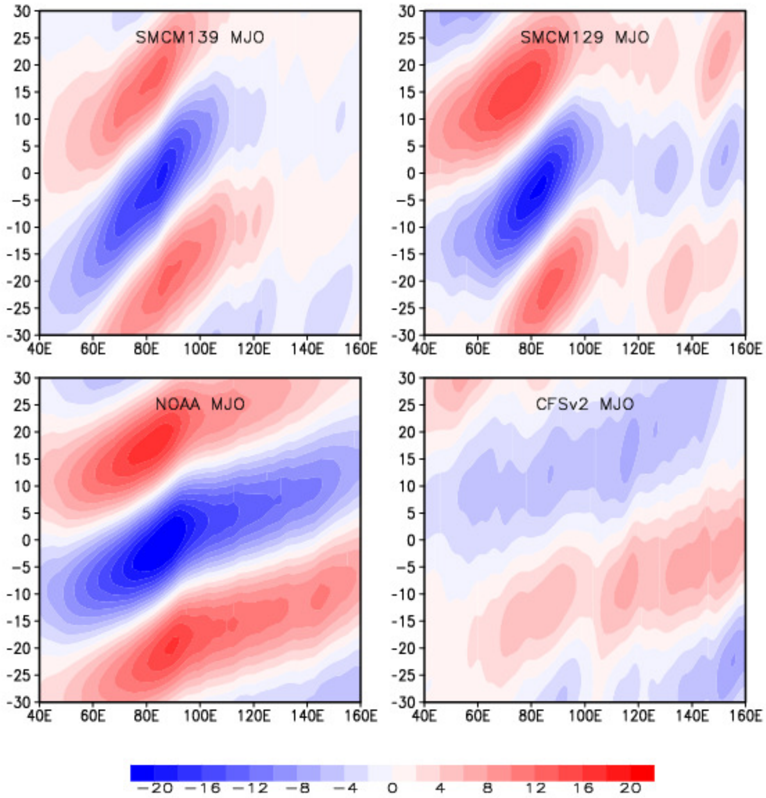

Figure 10. Hovmöller (averaged from 5°S - 5°N) plots showing MJO propagation for the MJO filtered OLR (W m^{-2}) anomalies.[Composite based on MJO peak over the box bounded by 82.5°E-90°E and Eq-8.5°N.]

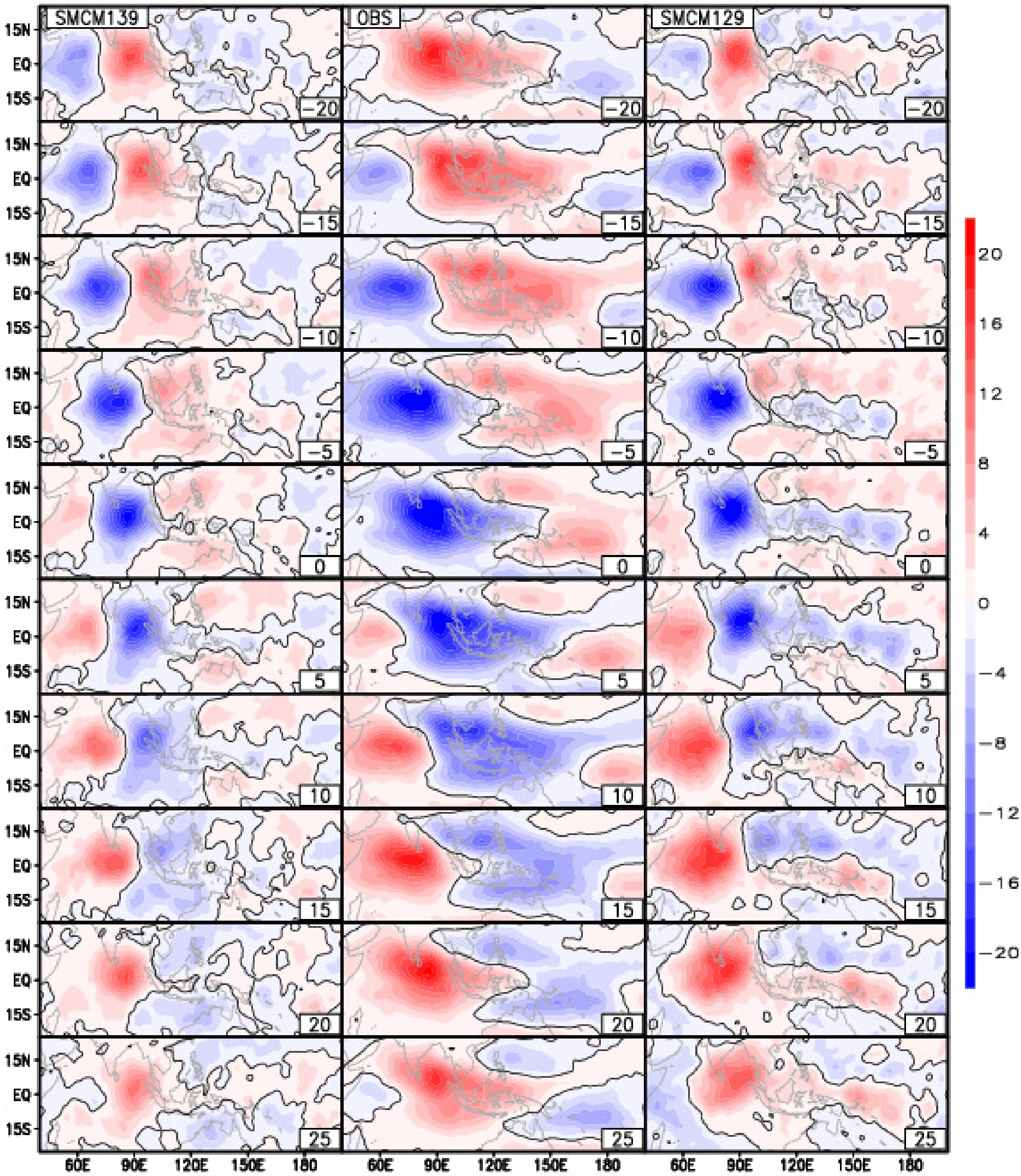

Figure 11. MJO Phase propagation. Composite of different phases of the MJO filtered OLR (W m^{-2}) anomalies constructed based on an MJO index averaged over 82.5°E-90°E and Eq-8.5°N. Run 139 are shown in the left hand side column, OBS in the middle and Run 129 in the right hand side column. Phase-lag stamps are seen in the right hand bottom corner.

it is of obvious curiosity to explore the MJO features in this run. Following the exact same methodology adopted to plot the Figures 2, 4 and 3 of *Goswami et al.* [2017c], we have plotted here the fields in Figures 9, 10 and 11, respectively. We note that in Figure 9, the MJO variance has somewhat deteriorated in Run 139. Particularly, the meridional span of the region of strong variance has narrowed, the variance over the Western Pacific has unrealistically strengthened and that over the California coast has weakened. The variance along the oceanic inter-tropical convergence zone towards the south of the Western Pacific, which was already poorly simulated in Run 129, has further worsened. Consistent with the observed limitation in the simulation of the MJO variance in Figure 9, the propagation features are also simulated with limited fidelity as seen from Figure 10. Although, both CFSsmcm runs are better compared to the CFSv2 simulated propagation features, it is debatable to claim for any improvement or its lack thereof in Run 139 compared to Run 129. Instead, it would be proper to say that both the CFSsmcm runs have their own strengths and weaknesses in simulating the MJO propagation features, especially passed the Maritime continent. A more detailed picture of the MJO propagation is shown in Figure 11, where the lag-lead composite of OLR anomalies, with respect the MJO peak defined over a box region in the Bay of Bengal (82.5°E-90°E and Eq-8.5°N), are plotted. Consistent with the results shown in Figure 10, the MJO structure is not as prominent as in the observations with a hint of a smaller spatial structure in the model simulations. Nevertheless, the simulated MJO structure in both the CFSsmcm runs, 129 and 139, looks significantly better than in CFSv2 MJO, shown on the bottom right corner of Figure 11.

3.5 Indian summer monsoon intra-seasonal oscillation (MISO)

Analogous to the TWK-spectra along the east-west direction in the tropics, the North-South version of the same diagram plotted for the boreal summer data over the Indian monsoon domain provides a first hand overview of the major modes of oscillation of the Indian summer monsoon (ISM). For the North-South TWK-spectra (Figure 12a, c and e), wavenumber 1 corresponds to 50 degrees of latitude (from 20°S to 30°N). As we had seen for the TWK-spectra in Figure 8, the North-South wavenumber-frequency spectra also has deteriorated in Run 139. Interestingly, the MISO power in the north-south spectra in Run 139 deteriorates whereas the seasonal mean precipitation improves. We need to recall here that, the SMCM parameter responsible for the stratiform convection decay time was found to be crucial for organization of convection in the CFSsmcm [*Goswami et al.*, 2017b] and MTD0

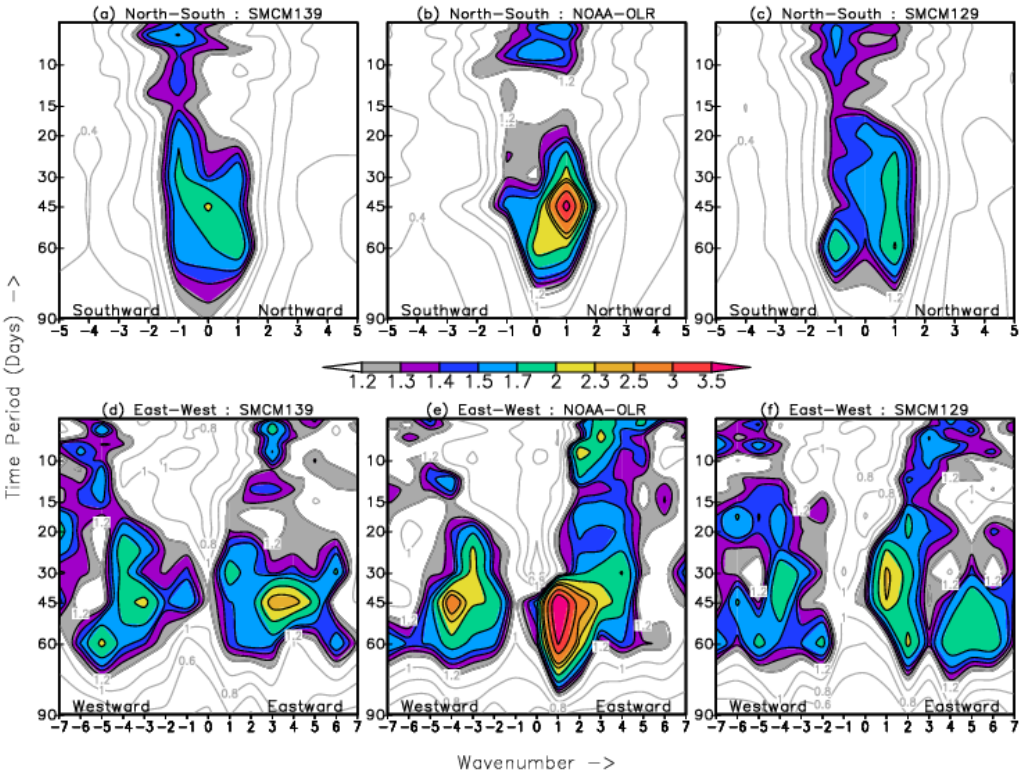

386 **Figure 12.** Wavenumber-frequency spectra of OLR (divided by the background red spectrum) computed
387 for the boreal summer season (JJAS). The top three panels show the north-south spectra (wavenumber 1 cor-
388 responds to the largest wave that exactly fits into 50°latitudes, from 20°S to 30°N; computed over 60°E to
389 100°E). The bottom three panels show the east-west spectra (wavenumber 1 corresponds to the length of the
390 equator).

is influential for controlling the mean precipitation only. So this is consistent with the formulation of the SMCM. Finding a balanced pair of values for MTD0 for continents/oceans and an adequate stratiform convection decay time scale to complement this pair of MTD0 values calls for further tuning of CFSsmcm parameters.

4 Discussion

We have run two different versions of the CFSsmcm model: one with one middle tropospheric dryness parameter (MTD0) value for the entire globe (Run 129) and the other with two separate values of MTD0 for continents and oceans (Run 139). For the sake of ease of discussion, let us call these two runs 129 and 139, as MTD_G and MTD_L/O, respectively. We performed some standard analyses to examine the difference in mean climate and its variability, based on 10-year long climate simulations. The motive behind doing this exercise is to highlight the sensitivity and resilience of the CFSsmcm, to changes in parameter values. Thereby exposing the scopes of improving the CFSsmcm model to the climate modeling community.

The CFSsmcm mean rainfall has already been demonstrated to be sensitive to the MTD0 parameter in *Goswami et al.* [2017b]. As a consequence the mean rainfall of the MTD_G and MTD_L/O runs are significantly different, especially over the rain abundant regions in the tropics, like, the Indian summer monsoon, West Pacific, Amazonia, etc. In the MTD_L/O run, the MTD0 values are chosen in such a way that the atmosphere over the continents trigger precipitation relatively quickly compared to that over the oceans. This adjustment has resulted in reducing the dry bias over the continents. As per our analyses, the simulation of the Indian summer monsoon (ISM) mean rainfall has improved the most in the MTD_L/O run. However, intra-seasonal variability has not shown much improvement. In fact, at times, it has worsened. The tropical wave spectrum (as seen from the TWK-diagram in Figure 8) looks a bit deteriorated in the MTD_L/O run. The same can be said for the MJO variability and propagation (Figures 10-12). As can be seen from Figure 12, power in the desired modes of variability of the ISM climate has also slightly deteriorated. The parameters responsible for organization of convection, especially the stratiform convection decay time parameter [*Goswami et al.*, 2017b], needs to be adjusted to suite the MTD_L/O run in order to simulate better intra-seasonal variability. However, the results obtained from this single attempt with a varying MTD0 look very encouraging. A thorough tunning of the CFSsmcm model for the MTD_L/O run bears promise to lead us to an even better version of the

CFSsmcm model with better seasonal mean rainfall and perhaps better intra-seasonal and synoptic scale variability.

References

Ajayamohan, R. S., B. Khouider, A. J. Majda, and Q. Deng (2016), Role of stratiform heating on the organization of convection over the monsoon trough, *Clim. Dyn.*, pp. 1–20, doi: 10.1007/s00382-016-3033-7.

Arakawa, A. (2004), The cumulus parameterization problem: Past, present, and future, *J. Clim.*, *17*(13), 2493–2525, doi:10.1175/1520-0442(2004)017<2493:RATCPP>2.0.CO;2.

Arakawa, A., and W. H. Schubert (1974), Interaction of a cumulus cloud ensemble with the large-scale environment, Part I, *J. Atmos. Sci.*, *31*(3), 674–701, doi:10.1175/1520-0469(1974)031<0674:IOACCE>2.0.CO;2.

Betts, A. K., and M. J. Miller (1986), A new convective adjustment scheme. Part II: Single column tests using GATE wave, BOMEX, ATEX and arctic air-mass data sets, *Quart. J. Roy. Met. Soc.*, *112*(473), 693–709, doi:10.1002/qj.49711247308.

Buizza, R., M. Milleer, and T. N. Palmer (1999), Stochastic representation of model uncertainties in the ECMWF ensemble prediction system, *Q. J. R. Meteorolog. Soc.*, *125*(560), 2887–2908, doi:10.1002/qj.49712556006.

Davini, P., J. von Hardenberg, S. Corti, H. M. Christensen, S. Juricke, A. Subramanian, P. A. G. Watson, A. Weisheimer, and T. N. Palmer (2016), Climate SPHINX: evaluating the impact of resolution and stochastic physics parameterisations in climate simulations, *Geosci. Model Dev. Discuss.*, *2016*, 1–29, doi:10.5194/gmd-2016-115.

De La Chevrotière, M., and B. Khouider (2017), A zonally symmetric model for the monsoon-Hadley circulation with stochastic convective forcing, *Theor. Comput. Fluid Dyn.*, *31*(1), 89–110, doi:10.1007/s00162-016-0407-8.

De La Chevrotière, M., Michèle, B. Khouider, and A. Majda (2015), Stochasticity of convection in Giga-LES data, *Clim. Dyn.*, *47*(5), 1845–1861, doi:10.1007/s00382-015-2936-z.

Deng, Q., B. Khouider, and A. J. Majda (2015), The MJO in a coarse-resolution GCM with a stochastic multicloud parameterization, *J. Atmos. Sci.*, *72*(1), 55–74, doi:10.1175/JAS-D-14-0120.1.

Deng, Q., B. Khouider, A. J. Majda, and R. S. Ajayamohan (2016), Effect of stratiform heating on the planetary-scale organization of tropical convection, *J. Atmos. Sci.*, *73*(1), 371–392, doi:10.1175/JAS-D-15-0178.1.

Dorrestijn, J., D. T. Crommelin, A. P. Siebesma, H. J. Jonker, and F. Selten (2016), Stochastic convection parameterization with Markov Chains in an intermediate-complexity GCM, *J. Atmos. Sci.*, *73*(3), 1367–1382.

Frenkel, Y., A. J. Majda, and B. Khouider (2012), Using the stochastic multicloud model to improve tropical convective parameterization: A paradigm example, *J. Atmos. Sci.*, *69*(3), 1080–1105, doi:10.1175/JAS-D-11-0148.1.

Frenkel, Y., A. J. Majda, and B. Khouider (2013), Stochastic and deterministic multicloud parameterizations for tropical convection, *Clim. Dyn.*, *41*(5-6), 1527–1551, doi:10.1007/s00382-013-1678-z.

Goswami, B. B., B. Khouider, R. P. M. Krishna, P. Mukhopadhyay, and A. J. Majda (2017a), Improving synoptic and intra-seasonal variability in CFSv2 via stochastic representation of organized convection, *Geophys. Res. Lett.*, *44*(2), 1104–1113, doi:10.1002/2016GL071542.

Goswami, B. B., B. Khouider, R. P. M. Krishna, P. Mukhopadhyay, and A. J. Majda (2017b), Implementation and calibration of a stochastic convective parameterization in the ncep climate forecast system, *J. Adv. Model. Earth Syst.*, p. submitted.

Goswami, B. B., B. Khouider, R. P. M. Krishna, P. Mukhopadhyay, and A. J. Majda (2017c), Improved tropical modes of variability in the Climate Forecast System model (version 2) via a stochastic multicloud model, *J. Atmos. Sci.*, doi:submitted.

Grabowski, W. W. (2001), Coupling cloud processes with the large-scale dynamics using the cloud-resolving convection parameterization (CRCP), *J. Atmos. Sci.*, *58*(9), 978–997, doi:10.1175/1520-0469(2001)058<0978:CCPWTL>2.0.CO;2.

Gregory, D., and P. R. Rowntree (1990), A mass flux convection scheme with representation of cloud ensemble characteristics and stability-dependent closure, *Mon. Weather Rev.*, *118*(7), 1483–1506, doi:10.1175/1520-0493(1990)118<1483:AMFCSW>2.0.CO;2.

Huffman, G. J., R. F. Adler, D. T. Bolvin, and E. J. Nelkin (2010), The TRMM multi-satellite precipitation analysis (TMPA), in *Satellite Rainfall Applications for Surface Hydrology*, pp. 3–22, Springer, doi:10.1007/978-90-481-2915-7_1.

Kain, J. S., and J. M. Fritsch (1990), A one-dimensional entraining/detraining plume model and its application in convective parameterization, *J. Atmos. Sci.*, *47*(23), 2784–2802, doi:10.1175/1520-0469(1990)047<2784:AODEPM>2.0.CO;2.

Kalnay, E., M. Kanamitsu, R. Kistler, W. Collins, D. Deaven, L. Gandin, M. Iredell, S. Saha, G. White, J. Woollen, Y. Zhu, A. Leetmaa, R. Reynolds, M. Chelliah, W. Ebisuzaki,

W. Higgins, J. Janowiak, K. C. Mo, C. Ropelewski, J. Wang, R. Jenne, and D. Joseph (1996), The NCEP/NCAR 40-Year reanalysis project, *Bull. Am. Meteorol. Soc.*, *77*(3), 437–471, doi:10.1175/1520-0477(1996)077<0437:TNYRP>2.0.CO;2.

Kasahara, A., and K. Puri (1981), Spectral representation of three-dimensional global data by expansion in normal mode functions, *Mon. Weather Rev.*, *109*(1), 37–51, doi: 10.1175/1520-0493(1981)109<0037:SROTDG>2.0.CO;2.

Khairoutdinov, M. F., and D. A. Randall (2001), A cloud resolving model as a cloud parameterization in the NCAR Community Climate System Model: Preliminary results, *Geophys. Res. Lett.*, *28*(18), 3617–3620, doi:10.1029/2001GL013552.

Khairoutdinov, M. F., S. K. Krueger, C.-H. Moeng, P. A. Bogenschutz, and D. A. Randall (2009), Large-eddy simulation of maritime deep tropical convection, *J. Adv. Model. Earth Syst.*, *1*(4).

Khouider, B., and A. J. Majda (2006), A simple multicloud parameterization for convectively coupled tropical waves. Part I: Linear analysis, *J. Atmos. Sci.*, *63*(4), 1308–1323, doi:10.1175/JAS3677.1.

Khouider, B., and A. J. Majda (2008), Multicloud models for organized tropical convection: Enhanced congestus heating, *J. Atmos. Sci.*, *65*(3), 895–914, doi:10.1175/2007JAS2408.1.

Khouider, B., A. J. Majda, and M. A. Katsoulakis (2003), Coarse-grained stochastic models for tropical convection and climate., *Proc. Natl. Acad. Sci. U.S.A.*, *100*(21), 11,941–6, doi: 10.1073/pnas.1634951100.

Khouider, B., J. Biello, and A. J. Majda (2010), A stochastic multicloud model for tropical convection, *Commun. Math. Sci.*, *8*(1), 187–216.

Khouider, B., A. St-Cyr, A. J. Majda, and J. Tribbia (2011), The MJO and convectively coupled waves in a coarse-resolution GCM with a simple multicloud parameterization, *J. Atmos. Sci.*, *68*(2), 240–264, doi:10.1175/2010JAS3443.1.

Kuo, H. L. (1965), On formation and intensification of tropical cyclones through latent heat release by cumulus convection, *J. Atmos. Sci.*, *22*(1), 40–63, doi:10.1175/1520-0469(1965)022<0040:OFAIOT>2.0.CO;2.

Liebmann, B., and C. Smith (1996), Description of a complete (Interpolated) outgoing longwave radiation dataset., *Bull. Am. Meteorol. Soc.*, *77*, 1275–1277.

Lin, J. W.-B., and J. D. Neelin (2000), Influence of a stochastic moist convective parameterization on tropical climate variability, *Geophys. Res. Lett.*, *27*(22), 3691–3694, doi: 10.1029/2000GL011964.

Lin, J. W.-B., and J. D. Neelin (2002), Considerations for stochastic convective parameterization, *J. Atmos. Sci.*, *59*(5), 959–975, doi:10.1175/1520-0469(2002)059<0959:CFSCP>2.0.CO;2.

Lin, J. W.-B., and J. D. Neelin (2003), Toward stochastic deep convective parameterization in general circulation models, *Geophys. Res. Lett.*, *30*(4), doi:10.1029/2002GL016203.

Majda, A. J., and B. Khouider (2002), Stochastic and mesoscopic models for tropical convection, *Proc. Natl. Acad. Sci. U.S.A.*, *99*(3), 1123–1128, doi:10.1073/pnas.032663199.

Palmer, T. (1996), On parameterizing scales that are only somewhat smaller than the smallest resolved scales, with application to convection and orography, in *Workshop on New Insights and Approaches to Convective Parametrization, 4-7 November 1996*, pp. 328–337, ECMWF, ECMWF, Shinfield Park, Reading.

Palmer, T. N. (2001), A nonlinear dynamical perspective on model error: A proposal for non-local stochastic-dynamic parametrization in weather and climate prediction models, *Q. J. R. Meteorolog. Soc.*, *127*(572), 279–304, doi:10.1002/qj.49712757202.

Peters, K., C. Jakob, L. Davies, B. Khouider, and A. J. Majda (2013), Stochastic behavior of tropical convection in observations and a multicloud model, *J. Atmos. Sci.*, *70*(11), 3556–3575, doi:10.1175/JAS-D-13-031.1.

Peters, K., T. Crueger, C. Jakob, and B. Möbis (2017), Improved MJO-simulation in ECHAM6.3 by coupling a stochastic multicloud model to the convection scheme, *J. Adv. Model. Earth Syst.*, doi:10.1002/2016MS000809.

Plant, R. S., and G. C. Craig (2008), A stochastic parameterization for deep convection based on equilibrium statistics, *J. Atmos. Sci.*, *65*, 87–105, doi: doi:10.1175/2007JAS2263.1.

Randall, D. A. (2013), Beyond deadlock, *Geophys. Res. Lett.*, *40*(22), 5970–5976, doi: 10.1002/2013GL057998.

Saha, S., S. Moorthi, H.-L. Pan, X. Wu, J. Wang, S. Nadiga, P. Tripp, R. Kistler, J. Woollen, D. Behringer, H. Liu, D. Stokes, R. Grumbine, G. Gayno, J. Wang, Y.-T. Hou, H.-Y. Chuang, H.-M. H. Juang, J. Sela, M. Iredell, R. Treadon, D. Kleist, P. Van Delst, D. Keyser, J. Derber, M. Ek, J. Meng, H. Wei, R. Yang, S. Lord, H. Van Den Dool, A. Kumar, W. Wang, C. Long, M. Chelliah, Y. Xue, B. Huang, J.-K. Schemm, W. Ebisuzaki, R. Lin, P. Xie, M. Chen, S. Zhou, W. Higgins, C.-Z. Zou, Q. Liu, Y. Chen, Y. Han, L. Cucurull, R. W. Reynolds, G. Rutledge, and M. Goldberg (2010), The NCEP Climate Forecast System reanalysis, *Bull. Am. Meteorol. Soc.*, *91*(8), 1015–1057, doi:

10.1175/2010BAMS3001.1.

Satoh, M., H. Tomita, H. Miura, S. Iga, and T. Nasuno (2005), Development of a global cloud resolving model a multi-scale structure of tropical convections, *J. Earth Simulator*, *3*(September), 11–19.

Schumacher, C., M. H. Zhang, and P. E. Ciesielski (2007), Heating structures of the TRMM field campaigns, *J. Atmos. Sci.*, *64*(7), 2593–2610, doi:10.1175/JAS3938.1.

Stachnik, J. P., C. Schumacher, and P. E. Ciesielski (2013), Total heating characteristics of the ISCCP tropical and subtropical cloud regimes, *J. Clim.*, *26*(18), 7097–7116, doi: 10.1175/JCLI-D-12-00673.1.

Takayabu, Y. N. (1994), Large-scale cloud disturbances associated with equatorial waves. Part II: Westward-propagating inertio-gravity waves, *J. Meteorol. Soc. Jpn.*, *72*(3), 451–465.

Teixeira, J., and C. A. Reynolds (2008), Stochastic nature of physical parameterizations in ensemble prediction: A stochastic convection approach, *Mon. Weather Rev.*, *136*(2), 483–496, doi:10.1175/2007MWR1870.1.

Troen, I. B., and L. Mahrt (1986), A simple model of the atmospheric boundary layer; sensitivity to surface evaporation, *Boundary Layer Meteorol.*, *37*(1), 129–148, doi: 10.1007/BF00122760.

Waite, M. L., and B. Khouider (2009), Boundary layer dynamics in a simple model for convectively coupled gravity waves, *J. Atmos. Sci.*, *66*(9), 2780–2795, doi: 10.1175/2009JAS2871.1.

Wheeler, M., and G. N. Kiladis (1999), Convectively coupled equatorial waves: Analysis of clouds and temperature in the wavenumber-frequency domain, *J. Atmos. Sci.*, *56*(3), 374–399, doi:10.1175/1520-0469(1999)056<0374:CCEWAO>2.0.CO;2.

Yanai, M., S. Esbensen, and J.-H. Chu (1973), Determination of bulk properties of tropical cloud clusters from large-scale heat and moisture budgets, *J. Atmos. Sci.*, *30*(4), 611–627.

Zhang, G., and N. A. McFarlane (1995), Sensitivity of climate simulations to the parameterization of cumulus convection in the canadian climate centre general circulation model, *Atmosphere-Ocean*, *33*(3), 407–446, doi:10.1080/07055900.1995.9649539.